ASTRONOMY & ASTROPHYSICS
SUPPLEMENT SERIES

Astron. Astrophys. Suppl. Ser. **125,** 573-580 (1997)

VLA polarimetry of compact steep spectrum sources

F. Mantovani[1], W. Junor[2], R. Fanti[1,3], L. Padrielli[1], and D.J. Saikia[4]

[1] Istituto di Radioastronomia del CNR, Bologna, Italy
[2] Institute for Astrophysics, University of New Mexico, Albuquerque NM, U.S.A.
[3] Dipartimento di Fisica, Universitá degli Studi, Bologna, Italy
[4] Tata Institute of Fundamental Research, National Centre for Radio Astrophysics, Pune 411 007, India

Received December 24, 1996; accepted February 12, 1997

Abstract. We present the polarization properties at sub-arcsecond resolutions of 8 Compact Steep-spectrum Sources (CSSs) observed with the VLA A-array at 5, 8.4 and 15 GHz. We find that the three most compact sources, two of which are unresolved and have an angular diameter < 100 milliarcsec are not polarized. Of the remaining 5, the two associated with quasars have prominent radio jets while the two galaxies and one unidentified object are dominated by their lobe emission. The components of these medium sized objects with median values of percentage polarization of about 9% at 5 GHz and 11% at 8.4 GHz, are more strongly polarized than the compact sources and do not show evidence of very large rotation measures.

Key words: galaxies: active — galaxies, quasars: radio polarization — interferometry

1. Introduction

The Compact Steep-spectrum Sources or CSSs are physically-small objects of sub-galactic dimensions. A large fraction of these, $\sim$ 70%, which have somewhat symmetric structure and have been named Compact Symmetric Objects, are believed to be the young precursors of the larger sized radio sources (Fanti et al. 1995; Readhead et al. 1996). A minority of CSSs shows a complex morphology or strongly asymmetric emission with respect to the core. The structures and sizes of these are probably affected by the ambient gas near the nucleus of the parent optical object (Pearson et al. 1985; Fanti et al. 1990; Saikia et al. 1995).

Most CSSs show low percentage polarizations (less than $\sim$ 1%) at or below 5 GHz (Saikia et al. 1987). The polarization properties of CSSs at frequencies above 5 GHz have been investigated recently by a number of authors (for example, see Junor et al. 1996 and references therein). Although several well-known members of this class have low rotation measure (RM), radio polarimetric surveys (Kato et al. 1987; Taylor et al. 1992; Inoue et al. 1995) have shown that many of the sources with high RM (> 700 rad m^{-2}) are CSSs. VLA observations by Mantovani et al. (1994) and Junor et al. (1996) on selected samples of CSSs have revealed several objects with large RM.

In this paper we present VLA A-array observations at 8.4 and 15 GHz of 8 CSSs, 3 of which are of subarcsec dimensions while the remaining 5 are medium sized objects. We derive their polarization properties, and compare these with our earlier observations of CSSs. These data complete the information about a sample of sources selected because there were indications (detection of low frequency variability, spectral index turnovers around 100 MHz) they were compact objects (Mantovani et al. 1992).

2. VLA observations

The VLA (Thompson et al. 1980) A-array observations were made in the X (8.4 GHz) and U (15 GHz) bands on 1990 September 10. The data were calibrated in the standard way using VLA calibrators and AIPS procedures. More detailed information on the data analysis can be found in Mantovani et al. (1994). Observations of the same sample of sources were done earlier at 5 GHz with the VLA A-array in 1986 May 30 (Mantovani et al. 1992). However, the polarization data were not presented earlier and are listed here along with the values at the higher frequencies.

3. VLA structure and polarimetry of CSSs

3.1. Derived values

The values and some of the properties of these sources estimated from the VLA A-configuration images at 5, 8.4 and 15 GHz are presented in Table 1. The contents of Table 1 are as follows: *Column 1*: source name; *Column 2*:

Send offprint requests to: F. Mantovani

Table 1. Observational parameters and observed properties

Source	Obs. ν MHz	Beam maj. $''$	Beam min. $''$	PA $^\circ$	σ_t mJy/b	σ_p mJy/b	C	R.A. (B1950) h m s	Dec.(B1950) $^\circ$ $'$ $''$	Flux peak mJy/b	Dens. total mJy
0320+053	4885	0.42	0.41	−76	0.10	0.16		03 20 41.54	05 23 34.6	705.6	715.2
	8440	0.27	0.27	47	0.06	0.07		41.54	34.2	413.9	466.9
	14940	0.18	0.14	66	0.10	0.20		41.52	34.3	157.8	201.5
0358+004	4885	0.41	0.40	65	0.3	0.2	a	03 58 33.36	00 28 11.2	246.6	311.8
							c	33.31	10.8	122.2	154.0
							d	33.12	08.6	3.2	5.9
	8440	0.30	0.28	51	0.07	0.06	a	33.35	11.3	144.4	209.5
							c	33.31	10.8	87.2	107.5
							d	33.11	08.7	1.0	4.5
0809−056	4885	0.43	0.37	−0.7	0.08	0.09	a	08 09 35.53	−05 40 19.3	186.2	303.6
							b	35.45	19.4	2.3	2.3
							c	35.19	20.2	85.4	151.2
	8440	0.24	0.23	37	0.02	0.03	a	35.51	19.6	79.8	170.8
							b	35.42	19.8	2.4	2.7
							c	35.17	20.5	45.3	80.2
	14490	0.13	0.12	42	0.06	0.13	a	35.52	19.6	23.6	66.6
							b	35.42	19.7	1.7	1.7
							c	35.17	20.5	18.5	27.1
1239−044	4885	0.43	0.38	−32	0.08	0.09	a	12 39 45.10	−04 29 51.2	60.2	336.8
							b	44.78	54.60	291.8	634.3
	8440	0.34	0.32	48	0.08	0.05	a	45.10	51.4	29.2	180.1
							b	44.82	54.7	158.8	332.0
	14490	0.12	0.12	45	0.10	0.18	a	45.08	51.0	3.5	72.5
							b	44.82	54.7	31.2	151.4
1422+202	4885	0.46	0.36	−76	0.08	0.12	a	14 22 37.47	20 14 00.5	65.2	157.1
							b	37.50	13 57.6	33.5	38.2
							c	37.48	54.8	14.0	31.0
							d	37.47	52.5	4.3	8.2
							e	37.50	49.5	193.6	319.6
							f	37.79	47.8	1.9	25.9
	8440	0.30	0.27	50	0.06	0.05	a	14 22 37.47	20 14 00.5	28.6	87.1
							b	14 22 37.51	13 57.5	26.6	27.0
							c	37.48	57.2	7.5	21.9
							d	37.48	52.45	2.5	5.0
							e	37.51	49.4	102.1	209.0
							f	37.76	47.9	0.8	17.4
	14940	0.17	0.15	50	0.12	0.21	a	14 22 37.47	20 14 00.4	5.8	18.5
							b	37.51	13 57.5	15.0	18.7
							c	37.49	54.7	1.6	2.1
							e	37.51	49.4	34.0	92.2
1741+279	8440	0.19	0.19	44	0.06	0.05	a	17 41 57.91	27 54 10.2	5.1	43.1
							b	57.89	04.8	73.3	81.9
							c	57.91	04.7	102.0	110.8
							d	58.01	00.9	0.6	6.3
	14490	0.17	0.16	47	0.10	0.18	a	57.91	10.3	1.9	5.7
							b	57.89	04.8	41.0	48.5
							c	57.91	04.7	164.9	170.7
2033+187	8440	0.34	0.21	75	0.04	0.05		20 33 18.03	18 46 40.1	174.0	178.8
	14940	0.19	0.13	70	0.10	0.22		18.03	40.0	75.0	75.2
2147+145	8440	0.35	0.22	78	0.04	0.06	a	21 47 59.30	14 35 44.7	369.1	378.8
							b	59.29	44.9	13.7	16.1
	14940	0.19	0.13	74	0.15	0.22	a	59.30	44.7	154.6	165.1
							b	59.28	45.0	4.3	4.6

the observing frequency in MHz; *Columns 3 to 5*: major axis, minor axis (both in arcsec) and the PA in degrees of the restoring beam major axis; *Column 6*: the rms noise in the total intensity map far from the source of emission; *Column 7*: − the rms noise $\sqrt{\sigma_Q^2 + \sigma_U^2}$, where σ_Q and σ_U are the rms noise on the blank sky in the distributions of the Stokes parameters Q and U; *Column 8* component label; *Columns 9 and 10*: RA and Dec. of the component peak; *Column 11*: peak flux density (mJy) of the component; *Column 12*: total flux density (mJy) of the component. The total intensity images at 5 GHz for the sources listed in Table 1 except for 1741+279, 2033+187 and 2147+145 were presented in Mantovani et al. (1992). However, observational parameters and derived properties obtained from the VLA observations at 5 GHz are incorporated in Table 1 to aid the reader.

Table 2. Polarization parameters

Source	O.I.	z	C	PA			RM	$RM\times$	%Pol			DP	DP
				6 cm	3.6 cm	2 cm		$(1+z)^2$	6 cm	3.6 cm	2 cm	6−3.6	3.6−2
0358+004	G	0.426	a	117 ± 2	115 ± 2		0	0	4.9	9.5		0.52	
0809−056			a	70±1	72±1	71±1	−7		9.5	10.9	11.3	0.87	0.96
			c	87±1	90±1	92± 1	−25		7.5	11.0	13.1	0.68	0.84
1239−044	G	0.480	a	86±1	88±1	90±1	−19	−42	13.5	14.7	[a]11.6	0.92	1.3
			b	2± 1	1± 2	−8± 2	24	52	2.3	3.7	5.3	0.62	0.70
1422+202	Q	0.871	a	26±6	33±3	42± 4	−75	−263	6.3	6.8	7.5	0.93	0.91
			b		112±1					0.8			
			c	104±1	108±1		−28	−98	34.2	34.2		1	
			d	96±1	102±1		−42	−147	39.0	63.3		0.62	
			e	150±3	160±3	156±1	−39	−137	10.2	10.9	[a]8.2	0.94	1.3
1741+279	Q	0.372	a		51±6					18.3			
			b		75±6	74±6	0	0		7.6	9.6		0.79
			c		42±5	35±5	135	254		4.0	[a]1.8		2.2

a: see notes on individual sources.

3.2. VLA polarimetry

The images obtained at 8.4 GHz and 15 GHz were convolved with a two-dimensional, circularly-symmetric Gaussian with a width of ∼0.4 arcsec. This approximates the resolution of the synthesized beam of the VLA A-array at 5 GHz. Parameters were calculated from the new images. Table 2 contains the following information: *Column 1*: source name; *Column 2*: optical identification; *Column 3*: the measured redshift; *Column 4*: component label; *Columns 5 to 7*: PA in degrees of the electric field vector at the peak of polarized emission (±1 rms error calculated from the distribution of PAs in a small box around the peak of polarized emission) at 5, 8.4 and 15 GHz respectively; *Column 8*: the Rotation Measure defined as $RM = \mathrm{d}\phi(\lambda)/\mathrm{d}(\lambda^2)$ in rad m^{-2}, where $\phi(\lambda)$ is the PA at wavelength λ. The RM is estimated by fitting the points with a linear least-squares fit; when computed between two frequencies RM suffers from an $n\pi$ ambiguity. *Column 9*: the RM corrected for redshift; *Columns 10 to 12*: polarization percentage at 5, 8.4 and 15 GHz respectively; *Columns 13 and 14*: the depolarization index, defined as the ratio of the fractional polarization at the longer wavelength to the fractional polarization at the shorter wavelength.

3.3. Notes on individual sources

3.3.1. 0320+053

This source appears, at best, to be only slightly resolved even at 15 GHz. At a redshift of 0.575 (Heckman et al. 1994), the linear diameter is <0.3 kpc (H_0 = 100 km s^{-1} Mpc^{-1}; q_0 = 1). There was no detection of polarized emission above the noise levels at any of the observing frequencies. The spectral index ($S \propto \nu^{-\alpha}$) ranges from $\alpha = 0.89$ between 5 and 8.4 GHz to $\alpha = 1.46$ between 8.4 and 15 GHz.

3.3.2. 0358+004 (3C 99)

The image obtained for 3C 99 at 8.4 GHz is presented in Fig. 1 and shows the well-known asymmetric triple structure (Mantovani et al. 1990). The 8.4 GHz image shows that the polarized emission comes mainly from component A. The jet region (i.e. the region between components A and C) is also slightly polarized with the magnetic field aligned with the jet axis. The 15 GHz data were affected by interference and are not presented here. In the earlier investigation of its structure by Mantovani et al. (1990), the A component was shown to contain a hot spot with a compact bright feature which has been detected in VLBI observations. Additionally, it was suggested that component C contains the nucleus.

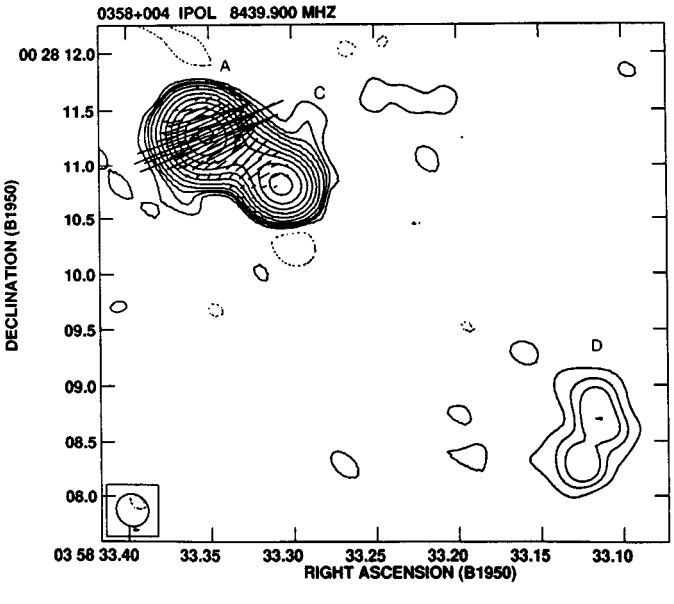

Fig. 1. VLA image of 0358+004 at 8.4 GHz. contours are at −0.2, 0.2, 0.4, 0.6, 1, 2, 4, 8, 16, 32, 64, 128, 256 mJy beam^{-1}. The peak flux density is 144.4 mJy beam^{-1}. A vector length of 1″= 10 mJy beam^{-1}

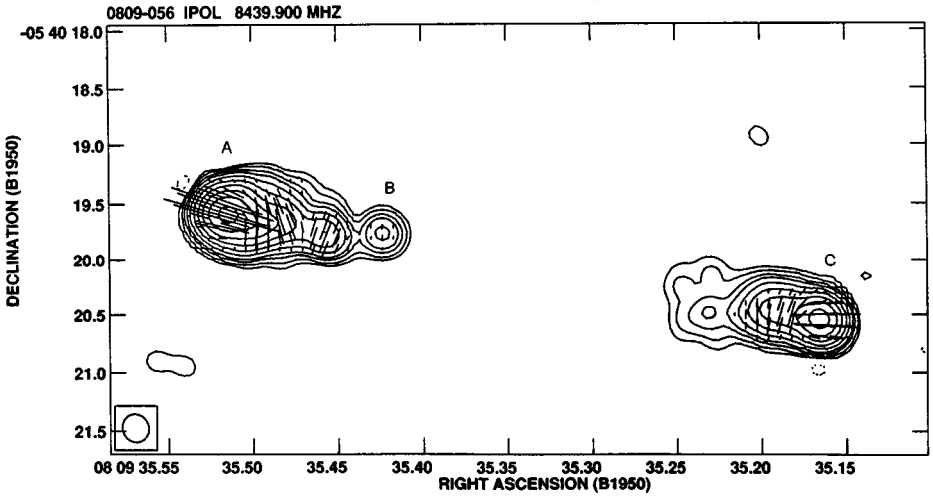

Fig. 2. VLA image of 0809−056 at 8.4 GHz. contours are at −0.15, 0.15, 0.3, 0.6, 1, 2, 4, 8, 16, 32, 64, 128 mJy beam^{-1}. The peak flux density is 79.8 mJy beam^{-1}. A vector length of 1″= 10 mJy beam^{-1}

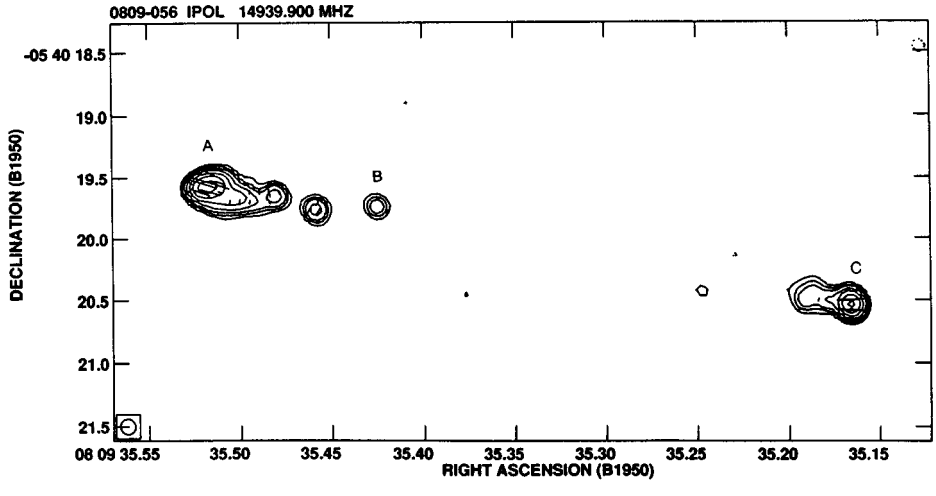

Fig. 3. VLA image of 0809−056 at 15 GHz. contours are at −0.3, 0.3, 0.6, 1, 2, 4, 8, 16, 32 mJy beam^{-1}. The peak flux density is 23.6 mJy beam^{-1}. A vector length of 1″= 12.5 mJy beam^{-1}

3.3.3. 0809−056

The two images obtained for 0809−056 at 8.4 GHz and 15 GHz (Figs. 2 and 3 respectively) confirm the double structure found at 5 GHz. The point-like component labelled B is likely to be the core of the source since it has a flat spectrum. It is also not polarized at the detection threshold of the present observations with an upper limit of about 3.5 per cent at 8.4 GHz. If this is the case, the source is asymmetric, with the further component (C) more depolarized, while going from shorter to longer wavelengths, and with a larger Faraday rotation than A. The more extended features in the lobes are not seen at $\lambda 2$ cm. The extended emission from the lobe, which is polarized at both $\lambda 6$ and $\lambda 4$ cm, is below the detection limits at $\lambda 2$ cm even in the image smoothed to the $\lambda 6$ cm resolution.

The magnetic field is aligned along the two components and suddenly changes direction by about 90° in the hot spots. The spectral indices of the two lobes are as steep as $1.3 - 1.4$.

3.3.4. 1239−044

This source shows a double lobed-structure that is asymmetric with a flux density ratio between the two lobes of about two, with lobe B being the brighter one. In Figs. 4 and 5 we present the 8.4 and 15 GHz images respectively. There is no indication of a component which could be the candidate for the nucleus. In the components, the ***E***-vectors suggest a circumferential field in the outer edges of the lobes but there are significant changes in the PAs of the vectors within the lobes. The Faraday rotation is

generally low, with values <100 rad m^{-2}, over the components. There is a suggestion of a large RM in the region around RA 12 39 44.85 and Dec $-$04 29 54.3 in lobe B with a value of about 440 rad m^{-2} in the source rest frame. However, this is close to one of the regions where the PAs change significantly across the lobe, and the high RM needs to be confirmed from more sensitive observations of higher resolution. The lobe A is heavily resolved at 15 GHz. The diffuse innermost part of the lobe is below the detection limit even in the smoothed image.

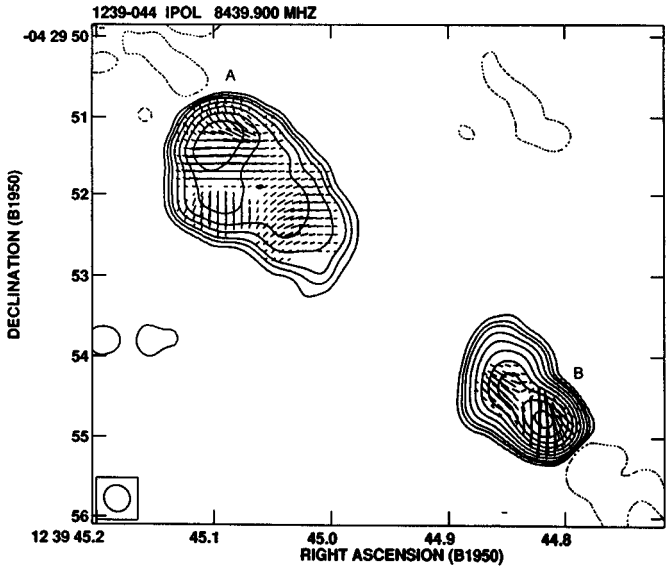

Fig. 4. VLA image of 1239−044 at 8.4 GHz. contours are at -0.3, 0.3, 0.6, 1, 2, 4, 8, 16, 32, 64, 128, 256 mJy beam^{-1}. The peak flux density is 158.8 mJy beam^{-1}. A vector length of 1″= 10 mJy beam^{-1}

3.3.5. 1422+202

This asymmetric source shows a long collimated one-sided jet. The core (component B) has a very low value of percentage polarization at 8 GHz (Fig. 6) which is likely to originate from the emerging part of the jet (see the 15 GHz image; Fig. 7). Polarized emission is detected all along the jet with the polarization percentage being as high as 30 − 60% in components C and D. The magnetic field looks quite ordered parallel to the jet axis and it changes direction in the hot spot (component E). The polarized emission at 15 GHz from component E is lower than those found at lower frequencies. The reason is possibly that the emission from that component, mainly along the ridge, is resolved out or below the sensitivity of these observations. The RM along the jet is never larger than 130 rad m^{-2} in the source rest frame. The lobe A on the counter-jet side is less polarized. Its emission is more diffuse and is located closer to the nucleus.

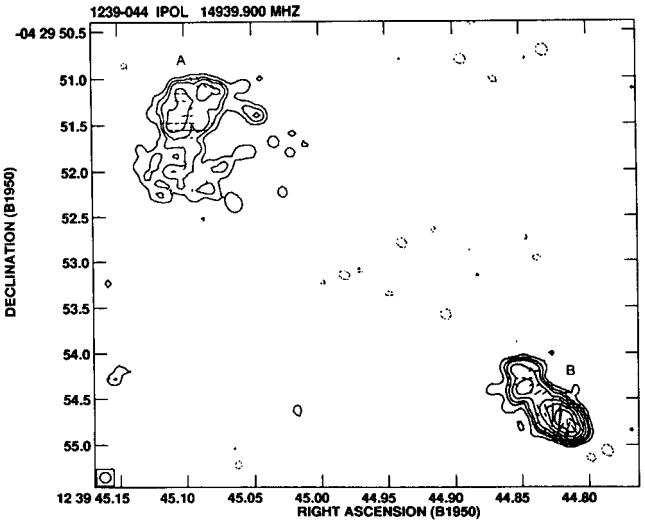

Fig. 5. VLA image of 1239−044 at 15 GHz. contours are at -0.3, 0.3, 0.6, 1, 2, 4, 8, 16, 32 mJy beam^{-1}. The peak flux density is 31.2 mJy beam^{-1}. A vector length of 1″= 12.5 mJy beam^{-1}

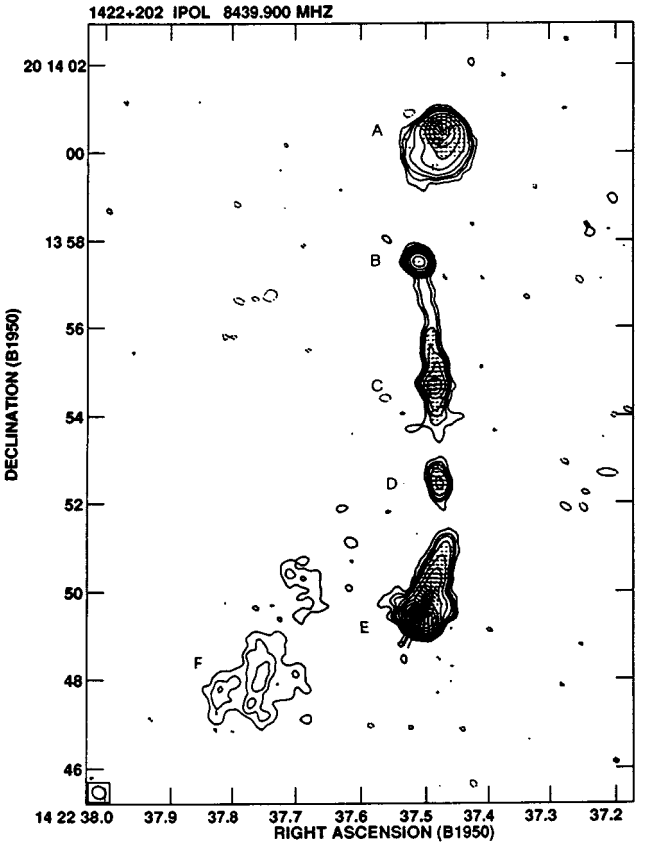

Fig. 6. VLA image of 1422+202 at 8.4 GHz. contours are at -0.2, 0.2, 0.4, 0.6, 1, 2, 4, 8, 16, 32, 64, 128 mJy beam^{-1}. The peak flux density is 102.1 mJy beam^{-1}. A vector length of 1″= 10 mJy beam^{-1}

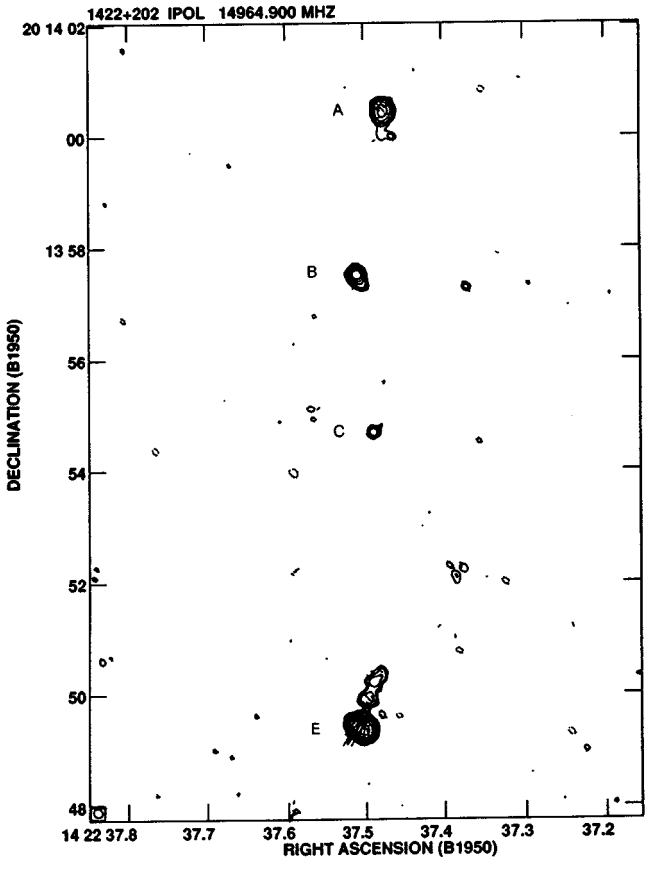

Fig. 7. VLA image of 1422+202 at 15 GHz. contours are at -0.3, 0.3, 0.6, 1, 2, 4, 8, 16, 32 mJy beam^{-1}. The peak flux density is 34.0 mJy beam^{-1}. A vector length of $1''$= 10 mJy beam^{-1}

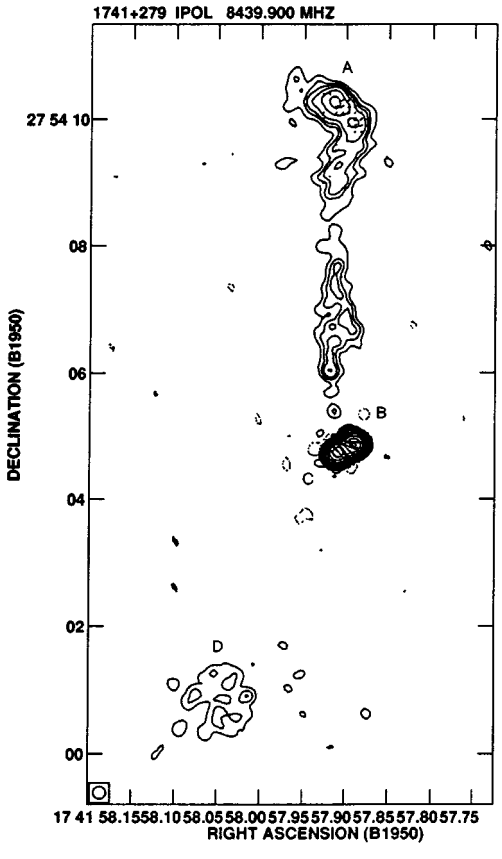

Fig. 8. VLA image of 1741+279 at 8.4 GHz. contours are at -0.2, 0.2, 0.4, 0.6, 1, 2, 4, 8, 16, 32, 64, 128 mJy beam^{-1}. The peak flux density is 100.4 mJy beam^{-1}. A vector length of $1''$= 10 mJy beam^{-1}

3.3.6. 1741+279

The image of this source at 8.4 GHz (Fig. 8) confirms the triple structure seen at 408 MHz in the MERLIN map by Mantovani et al. (1992). At 15 GHz (Fig. 9) we detect only the central components and the hot spot at the end of the northern jet. The central component is resolved in the VLA observations at higher resolution. The C component has an inverted spectral index and is likely to host the nucleus of the source although it has polarized emission. The component B exhibits marginal depolarization between 15 GHz to 8.4 GHz while component C is more stongly polarized at the lower frequency. However, the values reported in Table 2 have to be taken with care since the two components are barely separated. Since the RMs of components B and C are consistent with small values, within the errors, the inferred magnetic field is initially along the line connecting the peaks of emission of the two components, and later changes direction gradually to point towards the northern component A. There appears to be a large bend in the jet close to the nucleus. The jet later points northwards and has a wiggling collimated structure.

3.3.7. 2033+187

The VLA observations confirm that 2033+187 is unresolved at the sub-arcsecond resolution scale. The emission is not polarized at the sensitivity level of these observations.

3.3.8. 2147+145

This source was found to be unresolved in previous VLA A-array observations at 5 GHz and elongated along PA 159° at 15 GHz (Cotton 1983). We detect a weak unresolved component north-west of the main component along a PA of 140° and separated from it by about 0.4 arcsec (Figs. 10 and 11). This new component has a steep spectral index ($\alpha \sim 1.8$) and lies off-axis by about 90° with respect to the axis of the VLBI jet (Cotton et al. 1984). No polarized emission was detected in either components.

4. Discussion

The data presented in this paper complete the information about a sample of small-sized sources

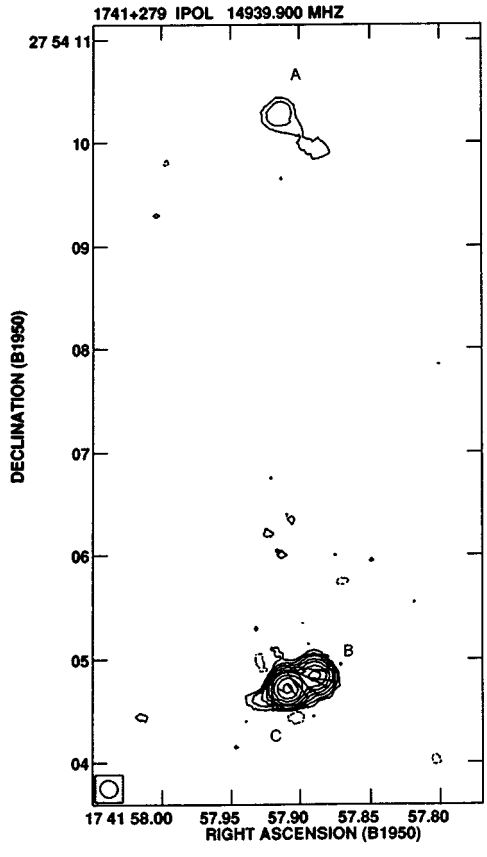

Fig. 9. VLA image of 1741+279 at 15 GHz. contours are at -0.4, 0.4, 0.6, 1, 2, 4, 8, 16, 32, 64, 128 mJy beam^{-1}. The peak flux density is 159.4 mJy beam^{-1}. A vector length of $1''$= 10 mJy beam^{-1}

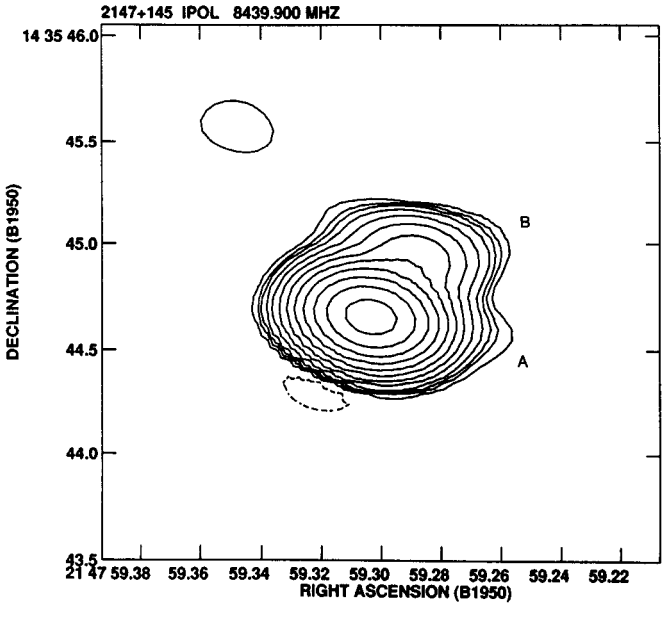

Fig. 10. VLA image of 2147+145 at 8.4 GHz. contours are at -0.2, 0.2, 0.4, 0.6, 1, 2, 4, 8, 16, 32, 64, 128, 256, 512 mJy beam^{-1}. The peak flux density is 369.1 mJy beam^{-1}

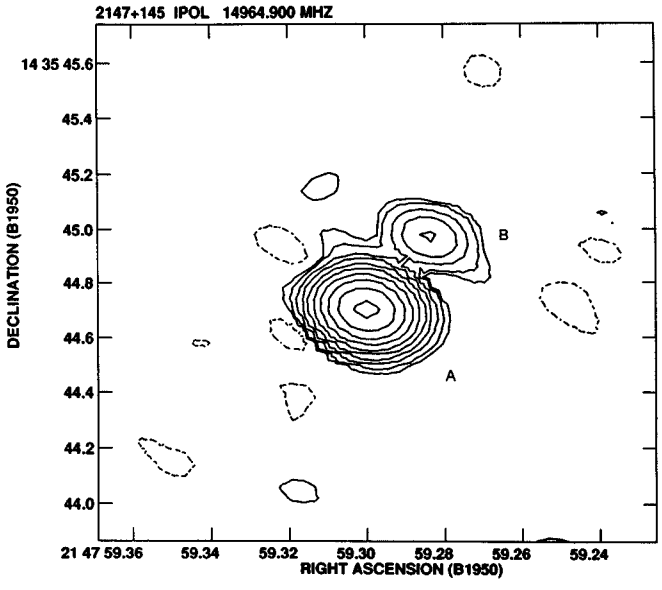

Fig. 11. VLA image of 2147+145 at 15 GHz. contours are at -0.2, 0.2, 0.4, 1, 2, 4, 8, 16, 32, 64, 128, 256 mJy beam^{-1}. The peak flux density is 154.6 mJy beam^{-1}

(Mantovani et al. 1992, 1994). The previous paper (Mantovani et al. 1994) presented the results on sources which were generally of small size and had high rotation measures. All but one of the sources discussed in that paper have a linear size < 14 kpc. The source 0725+147 is larger with a projected linear size of 25 kpc, and was found to have rotation measures of about +545 and -2576 rad m^{-2} for the two lobes in the rest frame of the source. This object is associated with a quasar at a redshift of 1.387 and has an absorption-line system at a similar redshift (Hewitt & Burbidge 1993).

Among the sources presented here, 0320+053, 2033+187 and 2147+145 are the most compact with the former two being unresolved with the VLA A-array at 15 GHz. This implies an angular dimension $<$100 mas, which corresponds to a linear size $<$0.3 kpc for $z = 0.5$. All of these are not polarized at the detection levels of these observations.

Two sources, 0809$-$056 and 1239$-$044, have an overall structure that is similar to 0725+147. However, unlike 0725+147, they do not show evidence of large rotation measure. The source 0358+004 also has a triple structure, which is much more asymmetric compared to the above group of objects. All of them have a linear size in the range $20 - 25$ kpc, a bit larger than the limit set by Fanti et al. (1995) for a steep spectrum source to be considered a member of the class of Compact Steep-spectrum Sources.

The two last sources in the sample, 1422+202 and 1741+279, each show a one-sided jet and an overall asymmetric structure, with a weak lobe of emission on the counter-jet side which is located closer to the nucleus. The

jets are knotty and the one in 1741+279 has a wiggling structure which deserves further investigation. Moreover, in the case of 1741+279 there is a clear indication of a large bend in the jet direction close to the component which is likely to host the nucleus.

The above five sources, including 0725+147, have a linear size which is somewhat larger (between about 21 and 43 kpc) than the "required" size of ≤ 15 kpc to be classified as CSSs. They can be interpreted as *medium sized objects* which are the more evolved versions of the CSSs, which are assumed to be *young* rather than frustrated objects (Fanti et al. 1995; Readhead et al. 1996).

We have summarized in Table 3 the overall polarization parameters derived for the five polarized sources of the group. It is worth mentioning that the percentage polarization of these sources is rather high (in the range of about $6-13\%$ at 8.4 GHz) and that they depolarize going from higher to lower frequencies. The percentage polarization is significantly higher than that found for the compact sources with high RM presented in Mantovani et al. (1994). The four compact sources show a percentage polarization <3, while only 0725+147 has a percentage polarization comparable to the above values. The fact that the percentage polarization shown by some of the components is sometimes lower at 15 GHz than at 8.4 GHz is probably due to the fact that the sensitivity of the observations to the low brightness emission was insufficient in those cases.

Table 3. Polarization parameters of the sources as a whole

Source	%Pol			DP	DP
	6 cm	3.6 cm	2 cm	6−3.6	3.6−2
0358+004	3.2	6.4		0.5	
0809−056	8.8	13.2	18.2	0.7	0.7
1239−044	6.2	8.3	8.1	0.7	1.0
1422+202	9.7	12.0	7.9	0.8	1.5
1741+279		8.5	3.4		2.5

Acknowledgements. The authors wish to think the referee, Dr. Ian W.A. Browne for his suggestions. FM thanks Miller Goss, Assistant Director, NRAO, Socorro, for his hospitality during period when part of the work was done. The National Radio Astronomy Observatory is operated by Associated Universities Inc., under cooperative agreement with the National Science Foundation; AIPS is NRAO's *Astronomical Image Processing System*.

References

Cotton W.D., 1983, ApJ 271, 51
Cotton W.D., Owen F.N., Geldzahler B.J., et al., 1984, ApJ 277, L41
Fanti R., Fanti C., Schilizzi R.T., et al., 1990, A&A 231, 333
Fanti C., Fanti R., Dallacasa D., et al., 1995, A&A 302, 317
Heckman T.M., O'Dea C.P., Baum S.A., Laurikainen E., 1994, ApJ 428, 65
Hewitt A., Burbidge G., 1993, ApJS 87, 451
Inoue M., Tabara H., Kato T., Aizu K., 1995, PASJ 47, 725
Junor W., Mantovani F., Peck A., et al., 1996, in: IAU Symposium No. 175, Ekers R., Fanti C., Padrielli L. (eds.)
Kato T., Tabara H., Inoue M., Aizu K., 1987, Nat 329, 223
Mantovani F., Saikia D.J., Browne I.W.A., et al., 1990, MNRAS 245, 427
Mantovani F., Junor W., Fanti R., et al., 1992, MNRAS 257, 353
Mantovani F., Junor W., Fanti R., et al., 1994, A&A 292, 59
Pearson T.J., Perley R.A., Readhead A.C.S., 1985, AJ 90, 738
Readhead A.C.S., Taylor G.B., Pearson T.J., Wilkinson P.N., 1996, AJ 460, 634
Saikia D.J., Singal A.K., Cornwell T.J., 1987, MNRAS 224, 379
Saikia D.J., Jeyakumar S., Wiita P.J., et al., 1995, MNRAS 276, 1215
Taylor G.B., Inoue M., Tabara H., 1992, A&A 264, 421
Thompson A.R., Clark B.G., Wade C.M., Napier P.J., 1980, ApJS 44, 151